PROCEEDINGS OF SCIENCE

Updates to the results of the Ultra-Heavy Cosmic Ray Analysis with CALET on the International Space Station

Wolfgang V. Zober,[a,*] **Brian F. Rauch,**[a] **Yosui Akaike**[b,c] **and Nicholas W. Cannady**[d] **for the CALET collaboration**

[a] *Department of Physics and McDonnell Center for the Space Sciences, Washington University, One Brookings Drive, St. Louis, Missouri 63130-4899, USA*

[b] *Waseda Research Institute for Science and Engineering, Waseda University, 17 Kikuicho, Shinjuku, Tokyo 162-0044, Japan*

[c] *Space Environment Utilization Center, Human Spaceflight Technology Directorate, Japan Aerospace Exploration Agency, 2-1-1 Sengen, Tsukuba, Ibaraki 305-8505, Japan*

[d] *Astroparticle Physics Laboratory, NASA/GSFC, Greenbelt, Maryland 20771, USA*

E-mail: wzober@wustl.edu

The Calorimetric Electron Telescope (CALET), launched to the International Space Station in August 2015 and continuously operating since, measures cosmic-ray (CR) electrons, nuclei, and gamma rays. CALET, with its 30 radiation length deep calorimeter, measures particle energy, allowing for the determination of primary and secondary nuclei spectra and secondary to primary ratios of the more abundant CR nuclei through $_{28}$Ni, while the main charge detector (CHD) can measure Ultra-Heavy (UH) CR nuclei up to and beyond $_{40}$Zr, with our recently accepted results to ApJ showing consistency with ACE-CRIS, SuperTIGER, and HEAO-3 through $_{44}$Ru. By using the special high-duty cycle (~90%) UH trigger in conjunction with a data selection cut that requires events to pass into the Total Absorption Calorimeter (TASC), we have leveraged energy information in our charge assignment routine. Simulations using Geant4 and EPICS are then used to evaluate data cuts in the analysis and corrections. In this ICRC, we will show how these flight simulations align with data, how analysis selection cuts have been made, and how a set of corrections for instrument systematics was produced.

39th International Cosmic Ray Conference (ICRC2025)
15–24 July 2025
Geneva, Switzerland

*Speaker

PoS(ICRC2025)165

1. Introduction

The CALorimetric Electron Telescope (CALET) on the International Space Station (ISS) is a Japanese led astroparticle observatory that was launched on August 19, 2015 and has been continously collecting scientific data since October 13, 2015. The main science objective of CALET is to directly measure the total cosmic-ray electron flux (e^-+e^+) to the highest energies (1 GeV to 20 TeV) with the main calorimeter (CAL), shown in the CALET instrument package in Fig. 1a. CALET is also capable of measuring gamma rays (10 GeV to 10 TeV) and cosmic-ray nuclei (up to 1,000 TeV). In addition, there is the CALET Gamma-ray Burst (GRB) Monitor (CGBM), which can make simultaneous observations with the calorimeter. As an instrument CALET has recorded over 4 billion events in total and over 2 billion above 10 GeV during operations.

The main instrument comprises three detector systems: the charge detector (CHD), imaging calorimeter (IMC), and the total absorption calorimeter (TASC), shown in more detail in Figs. 1a and 1b. The CHD on top of CALET is comprised of two layers of 14 scintillator paddles (oriented in x and y layers). Each scintillator paddle is 32 mm wide by 10 mm thick by 450 mm long. The IMC is underneath the CHD, and is 156.5 mm tall and made of 8 layers of both x and y scintillating fibers that are 1 mm wide squares and 448 mm long. In between each x-y pair of fiber layers in the IMC is a combined 3.0 radiation lengths (X_0) of tungsten arranged such that the first 5 layers are $0.2X_0$ thick and the bottom two are $1.0X_0$ thick. At the bottom of the instrument stack is the TASC. The TASC is made of 6 x and y layers of 16 lead tungstate (PWO) scintillator logs. Each of these logs are 19 mm wide, 20 mm tall, and 326 mm long. Combined these logs give the TASC a total depth of $27X_0$.

For this analysis, the CHD provides the primary particle charge identification. All three detectors are utilized for track reconstruction, but this is primarily based on the IMC, while the particle energy is determined from the calorimeters, with determination based primarily on TASC measurements.

CALET utilizes a number of trigger schemes based on minimum signal at different points of the detector. There are three simultaneously active hardware triggers: single particle, low-energy, and

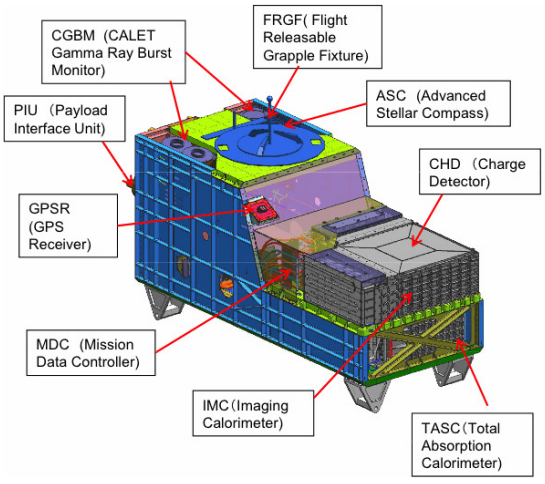

Figure 1(a): CALET instrument package detailing locations of the various CALET subsystems.

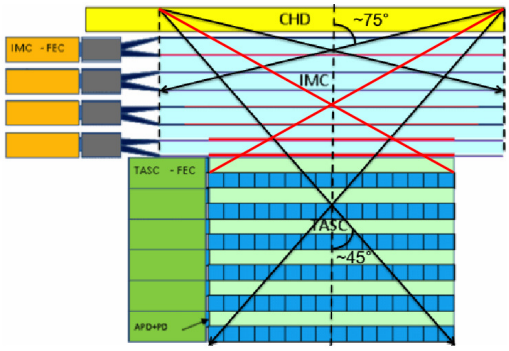

Figure 1(b): CALET side-view showing CHD, IMC, and TASC detector placement with the maximum acceptance angles for detection. The maximum acceptance angle (75°) for the UH trigger analysis is shown in black and in red for the TASC analysis (45°).

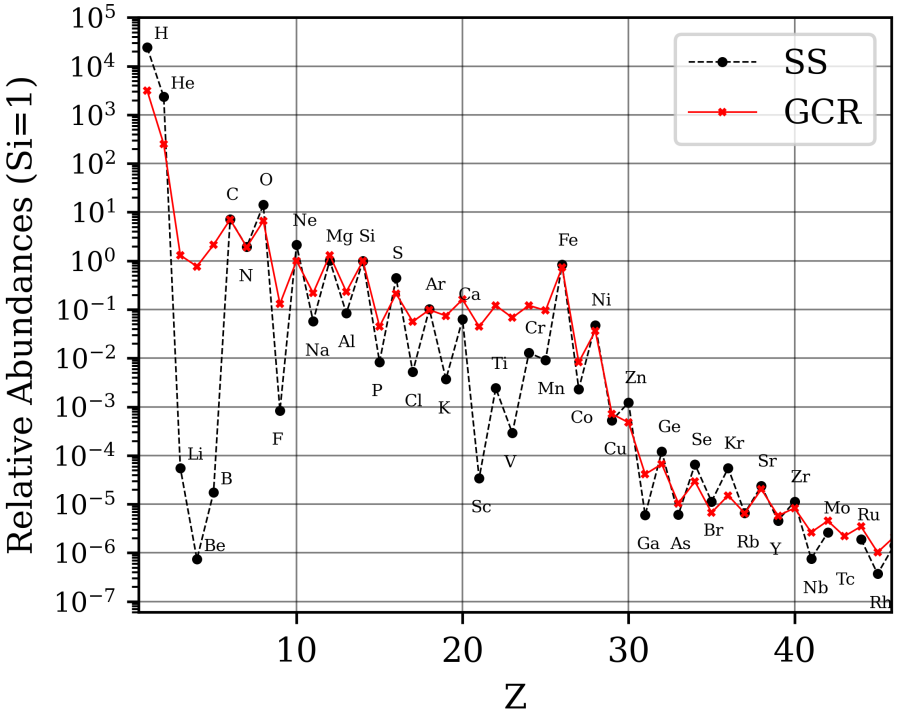

Figure 2: Solar System (SS) [1] and Galactic cosmic-ray (GCR) relative abundances at 2 GeV/nuc. The red line depicts average GCR data, sourced for 1≤Z≤2 from [2], Z=3 from [3], 4≤Z≤15 from [4], and 16≤Z≤45 from [5] normalized to $_{14}$Si.

high-energy. Run modes are configured for these hardware triggers (except the high-energy shower mode, which is always active for CALET primary science) via flight-configurable discriminator thresholds. The Ultra-Heavy (UH) trigger mode used in this analysis requires a high threshold in the CHD and does not require passage through the lower half of the IMC or the top of the TASC.

2. Ultra-Heavy Cosmic Rays

The measurement of ultra-heavy Galactic cosmic rays (UHGCR), $_{30}$Zn and higher charge elements, provides insight into the origins of cosmic rays. In Fig. 2, the relative abundances of cosmic rays elements ($1 \leq Z \leq 45$) with energies of 2 GeV/nucleon are compared to the Solar System (SS) abundances normalized to $_{14}$Si [1, 2, 3, 4, 5]. These two samples of Galactic matter are nominally consistent, with most of the differences accounted for by cosmic ray spallation between source and detection and by acceleration efficiencies. In the cosmic rays we see that $_{26}$Fe is $\sim 5\times10^3$ times less abundant than $_1$H, and that the UHGCR with charges $30 \leq Z \leq 40$ are $\sim 10^5$ times less abundant than $_{26}$Fe. Single-element resolution UHGCR measurements have so far only been made by a small number of instruments. Balloon-borne measurements go up to $_{40}$Zr by TIGER [6] and up to $_{56}$Ba by SuperTIGER [7] at ~GeV/nuc energies, while the single element space-based measurements go up to $_{38}$Zr by the ACE-CRIS [8] instrument at hundreds of MeV/nuc and our recently accepted results in [9] go up to $_{44}$Ru.

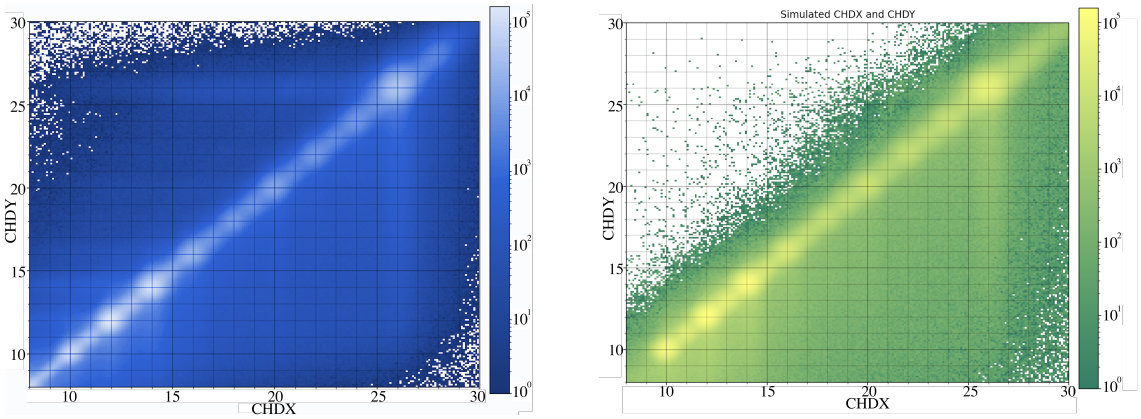

Figure 3: CHDX-CHDY charge consistency plots. Left figure shows real data taken by the UH trigger on CALET. Right figure shows the simulated data scaled to match abundances.

3. Analysis Methods

The results to be published in ApJ[9] reflect data from October 2015 to end of November 2023, approximately 8 years of operations. For data quality purposes, all events must meet signal thresholds for the UH-trigger and must not occur on the edges of CHDX and CHDY as those regions of the detector suffer from lower statistics and prevents spatial corrections from being applied with high fidelity. Data that correspond to times when the ISS is reoriented is also removed from the final dataset. The analysis process will then perform additional selection cuts based on minimum deposited energy, charge consistency, location of events, and interactions within the field of view.

Several secondary UH calibrations for optimizing the UH region of charge are also performed. These are multiplicative correction factors that rely on average signal from $_{10}$Ne, $_{12}$Mg, $_{14}$Si, and $_{26}$Fe to generate a 4 peak average correction factor for event location in CHD and in time (bins of one week over the lifetime of CALET). Charge assignment is then done by binning over bins of deposited energy using a Tarle model fit in each deposited energy bin that uses the peak positions for $6 \leq Z \leq 28$ and the expected charge number for CHDX and CHDY. To give constraints on the model fits and prevent misassigned charge numbers in the UH regime, the Tarle routine has strict rules on the maxima and minima of parameters to keep resulting equations and expected peak positions for $Z > 30$ consistent with the fits used in the CALET $_{26}$Fe and $_{28}$Ni analyses [10, 11].

4. Use of Simulations

To correct for species- and energy-dependent losses caused by data selection cuts, Monte Carlo simulations have been done with the EPICS [12] package, using DPMJET-III [13] for hadronic interactions and a detailed instrument mass model. Events were generated for species $_{10}$Ne to $_{39}$Y over 1 GeV-550 GeV, and the data selections are applied as in the flight data analysis. From this, one can calculate the survival fraction for each species in the analysis. These events are then scaled to match the abundance and noise profile of observed events by CALET. (Figure 3) As the measurement of abundances is done without determination of event energy, it is required that we use the spectral shape of each species to propagate the energy-dependent efficiencies for a scaling factor

appropriate for our result. These elemental fluxes are taken from a combination of ACE-CRIS[14] and HEAO-3-C2[4] for $_{10}$Ne through $_{26}$Fe, and we assume the spectral shape of $_{26}$Fe for heavier elements.

This correction factor is derived for each species as the ratio of the flux multiplied by the efficiency integrated over the energy range of interest to the flux multiplied by the efficiency integrated over the entire energy range.

The interaction rate in EPICS simulations is based on the cross-sections of interacting nuclei. However, the cross sections for the majority of UH nuclei in CALET's energy range are not measured, so cross sections must be modeled based on nuclear processes, A, Z, nuclear radii, and energy. To determine the systematic impact of relying on EPICS and DPMJET simulations, additional simulations and analytical methods were used.

These additional simulations were performed with two different packages in Geant4 [15]. The default Geant4 simulation uses the shielding physics list but the default radius function is a piecewise function that results in a large break in particle radii that is not consistent with the other simulation packages or analytical models.

$$R(A) \approx \begin{cases} r_0 A^{1/3}(1 - A^{-2/3}) & \text{if } A \leq 50, \\ r_0 A^{0.27} & \text{if } A \geq 50. \end{cases} \tag{1}$$

This break can be seen in Figure 4, where the piecewise discontinuity in the radii occurs at around Z=22. To resolve this break, the default Geant4 radii was was swapped out with two alternative functions. The first is the RMS charge radii within Geant4,

$$R(A) = 1.24 * A^{0.28} \tag{2}$$

The other function is based on the radii function that is used in the DPMJET code. While not explicitly shown in Figure 4, it is similar to Nilsen's model [16] which expects

$$R(A) = r_0 * A^{1/3} \tag{3}$$

In DPMJET, r_0 is 1.12 and in Nilsen et al values for r_0 vary between 1.2 and 1.3. The differences between these simulations do vary in more ways than just this, as the calculations of the cross sections and interactions vary based on the nuclear physics processes deemed to be relevant to that simulation code base for that particular and energy.

These simulations are then used to determine an example survival fraction through a sample of material. For this work the first layer of the CHD is used, which is 1 cm of EJ-204, polyvinyltoluene. Additionally, these survival fraction simulations are compared to an analytical method that uses the average path length traversed within the material and the interaction mean free paths for each Z. The total charge-changing sections used for mean-free path calculations come from [16].

The resultant survival fractions are shown in Fig. 5a. By taking the inverse of the survival fractions and normalizing to $_{26}$Fe, differences in scaling factors can be neglected and distinct trendlines between individual models can be seen in Fig. 5b. These inverse survival fractions can then be used as a source of systematic error on the analysis.

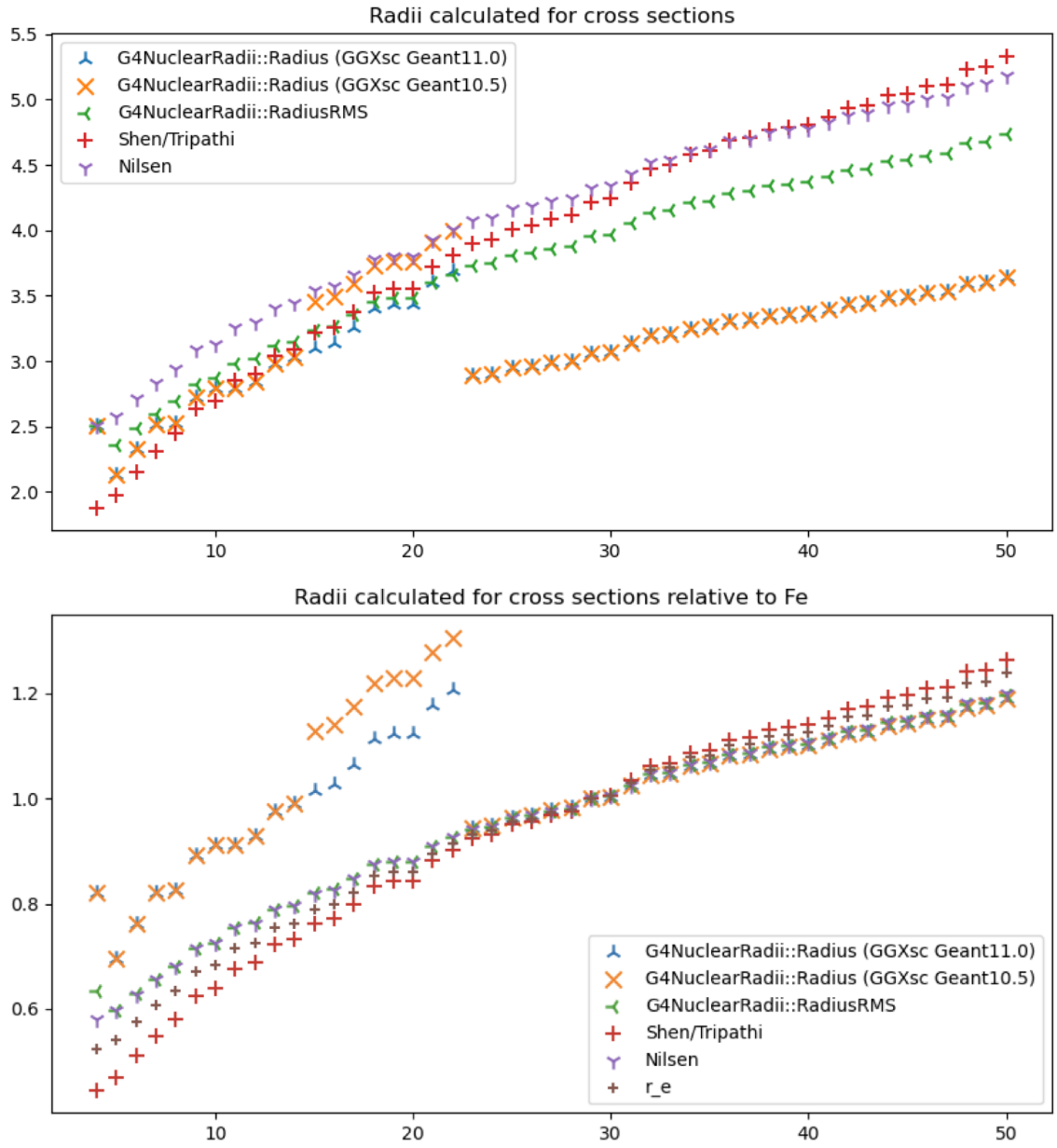

Figure 4: Radii of different cross-section models used in simulations. Top figure shows raw values as a function of Z. Y-axis is in arb. units. Bottom figure shows these radii relative to $_{26}$Fe.

5. Results

This work allows CALET to produce results that are in good agreement with the results from other experiments. (Data to be found in [9]) In Fig. 6, the CALET UH abundances for $14 \leq Z \leq 44$ are compared to HEAO, SuperTIGER, and ACE-CRIS abundances. While CALET's elemental abundances are not unique in this range, they do provide a check on other UH measurements. The significant overlap with the SuperTIGER energy range with different systematics makes this comparison particularly significant through Z = 44.

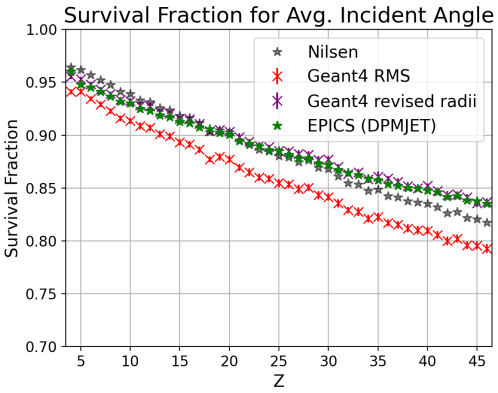

Figure 5(a): Survival fractions as determined by simulations in EPICS and Geant4, and the analytical model from Nilsen (Figure published in ApJ [9] under a Creative Commons Attribution (CC BY) license.)

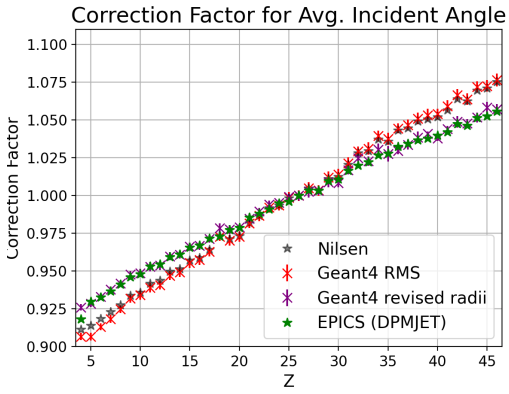

Figure 5(b): The derived correction factors from the survival fractions relative to $_{26}$Fe. (Figure published in ApJ under a Creative Commons Attribution (CC BY) license.)

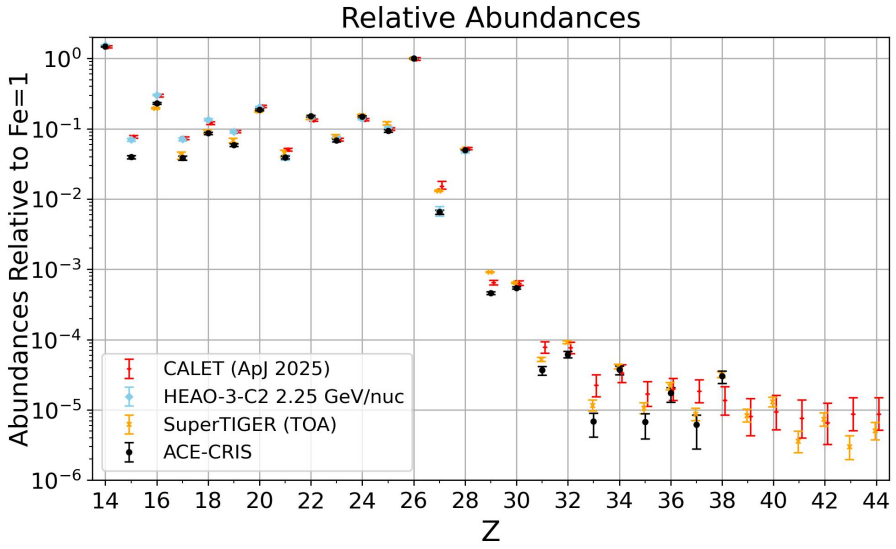

Figure 6: (Data published in ApJ [9] under a Creative Commons Attribution (CC BY) license.) Abundances of the elements relative to $_{26}$Fe for CALET with comparison to ACE-CRIS, HEAO-3-C2, and SuperTIGER.

However, the statistics for Z > 28 events do not yet allow reliable fits. With CALET expected to continue through the end of the ISS, greater statistics from the extended operations will provide the opportunity to revisit this analysis with a significantly improved UH data set and allow for better statistical resolution on the fitting routine and higher accuracy in the energy binning. There are additional ideas on how to modify the binning for the Tarle charge assignment model to better constrain low energy events. Additionally, future work will attempt an HE-trigger analysis which could determine the abundances of all Z in CALET's range. This secondary analysis with an alternative trigger would also allow exploration into potential Z-dependencies in trigger efficiencies and sampling biases as a function of Z based on rigidity-selections and interaction fraction.

6. Acknowledgements

We gratefully acknowledge JAXA's contributions to the development of CALET and to the operations aboard the JEM-EF on the ISS. This work was supported in part by JSPS Grant-in-Aid for Scientific Research (S) No. 26220708, No. 19H05608, and No. 24H00025, JSPS Grant-in-Aid for Scientific Research (B) No. 24K00665, and by the MEXT Supported Program for the Strategic Research Foundation at Private Universities (2011-2015) (No. S1101021) at Waseda University. The CALET effort in Italy is supported by ASI under Agreement No. 2013-018-R.0 and its amendments. The CALET effort in the United States is supported by NASA through Grants No. NNX16AB99G, No. NNX16AC02G, and No. NNH14ZDA001N-APRA-0075.

References

[1] K. Lodders. *The Astrophysical Journal*, 519:1220–1247, 2003.

[2] T. Sanuki et al. *The Astrophysical Journal*, 545(2):1135–1142, 2000.

[3] M. Aguilar et al. *The Astrophysical Journal*, 736(2):105, 105, 2011. DOI: 10.1088/0004-637X/736/2/105.

[4] J. J. Engelmann et al. *Astronomy & Astrophysics*, 233:96–111, 1990.

[5] N. E. Walsh. PhD thesis, Washington University in St. Louis, 2020.

[6] B. F. Rauch et al. *The Astrophysical Journal*, 697(2):2083–2088, 2009.

[7] N. E. Walsh et al. *Advances in Space Research*, 70(9):2666–2673, 2022. DOI: 10.1016/j.asr.2022.04.063.

[8] W. R. Binns et al. *ApJ*, 936(1):13, 13, 2022. DOI: 10.3847/1538-4357/ac82e7.

[9] O. Adriani et al. *The Astrophysical Journal*, 2025. DOI: https://doi.org/10.3847/1538-4357/ade3cc.

[10] O. Adriani et al. *Phys. Rev. Lett.*, 126:241101, 24, 2021. DOI: 10.1103/PhysRevLett.126.241101.

[11] O. Adriani et al. *Phys. Rev. Lett.*, 128:131103, 13, 2022. DOI: 10.1103/PhysRevLett.128.131103.

[12] K. Kasahara. In *24th International Cosmic Ray Conference*, volume 1 of *International Cosmic Ray Conference*, page 399, 1995.

[13] S. Roesler, R. Engel, and J. Ranft. In A. Kling et al., editors, *Advanced Monte Carlo for Radiation Physics, Particle Transport Simulation and Applications*, pages 1033–1038, Berlin, Heidelberg. Springer Berlin Heidelberg, 2001.

[14] K. A. Lave et al. *The Astrophysical Journal*, 770:117, 2013.

[15] J. Allison et al. *Nuclear Instruments and Methods in Physics Research Section A: Accelerators, Spectrometers, Detectors and Associated Equipment*, 835:186–225, 2016. DOI: https://doi.org/10.1016/j.nima.2016.06.125.

[16] B. S. Nilsen et al. *Physical Review C*, 52(6):3277–3290, 1995.

Full Author List: CALET Collaboration

O. Adriani,[1,2] Y. Akaike,[3,4] K. Asano,[5] Y. Asaoka,[5] E. Berti,[2,6] P. Betti,[2,6] G. Bigongiari,[7,8] W.R. Binns,[9] M. Bongi,[1,2] P. Brogi,[7,8] A. Bruno,[10] N. Cannady,[11] G. Castellini,[6] C. Checchia,[7,8] M.L. Cherry,[12] G. Collazuol,[13,14] G.A. de Nolfo,[10] K. Ebisawa,[15] A. W. Ficklin,[12] H. Fuke,[15] S. Gonzi,[1,2,6] T.G. Guzik,[12] T. Hams,[16] K. Hibino,[17] M. Ichimura,[18] M.H. Israel,[9] K. Kasahara,[19] J. Kataoka,[20] R. Kataoka,[21] Y. Katayose,[22] C. Kato,[23] N. Kawanaka,[24,25] Y. Kawakubo,[26] K. Kobayashi,[3,4] K. Kohri,[25,27] H.S. Krawczynski,[9] J.F. Krizmanic,[11] P. Maestro,[7,8] P.S. Marrocchesi,[7,8] M. Mattiazzi,[13,14] A.M. Messineo,[8,28] J.W. Mitchell,[11] S. Miyake,[29] A.A. Moiseev,[11,30,31] M. Mori,[32] N. Mori,[2] H.M. Motz,[33] K. Munakata,[23] S. Nakahira,[15] J. Nishimura,[15] M. Negro,[12] S. Okuno,[17] J.F. Ormes,[34] S. Ozawa,[35] L. Pacini,[2,6] P. Papini,[2] B.F. Rauch,[9] S.B. Ricciarini,[2,6] K. Sakai,[36] T. Sakamoto,[26] M. Sasaki,[11,30,31] Y. Shimizu,[17] A. Shiomi,[37] P. Spillantini,[1] F. Stolzi,[7,8] S. Sugita,[26] A. Sulaj,[7,8] M. Takita,[5] T. Tamura,[17] T. Terasawa,[5] S. Torii,[3] Y. Tsunesada,[38,39] Y. Uchihori,[40] E. Vannuccini,[2] J.P. Wefel,[12] K. Yamaoka,[41] S. Yanagita,[42] A. Yoshida,[26] K. Yoshida,[19] and W. V. Zober[9]

[1]Department of Physics, University of Florence, Via Sansone, 1 - 50019, Sesto Fiorentino, Italy [2]INFN Sezione di Firenze, Via Sansone, 1 - 50019, Sesto Fiorentino, Italy [3]Waseda Research Institute for Science and Engineering, Waseda University, 17 Kikuicho, Shinjuku, Tokyo 162-0044, Japan [4]Space Environment Utilization Center, Human Spaceflight Technology Directorate, Japan Aerospace Exploration Agency, 2-1-1 Sengen, Tsukuba, Ibaraki 305-8505, Japan [5]Institute for Cosmic Ray Research, The University of Tokyo, 5-1-5 Kashiwa-no-Ha, Kashiwa, Chiba 277-8582, Japan [6]Institute of Applied Physics (IFAC), National Research Council (CNR), Via Madonna del Piano, 10, 50019, Sesto Fiorentino, Italy [7]Department of Physical Sciences, Earth and Environment, University of Siena, via Roma 56, 53100 Siena, Italy [8]INFN Sezione di Pisa, Polo Fibonacci, Largo B. Pontecorvo, 3 - 56127 Pisa, Italy [9]Department of Physics and McDonnell Center for the Space Sciences, Washington University, One Brookings Drive, St. Louis, Missouri 63130-4899, USA [10]Heliospheric Physics Laboratory, NASA/GSFC, Greenbelt, Maryland 20771, USA [11]Astroparticle Physics Laboratory, NASA/GSFC, Greenbelt, Maryland 20771, USA [12]Department of Physics and Astronomy, Louisiana State University, 202 Nicholson Hall, Baton Rouge, Louisiana 70803, USA [13]Department of Physics and Astronomy, University of Padova, Via Marzolo, 8, 35131 Padova, Italy [14]INFN Sezione di Padova, Via Marzolo, 8, 35131 Padova, Italy [15]Institute of Space and Astronautical Science, Japan Aerospace Exploration Agency, 3-1-1 Yoshinodai, Chuo, Sagamihara, Kanagawa 252-5210, Japan [16]Center for Space Sciences and Technology, University of Maryland, Baltimore County, 1000 Hilltop Circle, Baltimore, Maryland 21250, USA [17]Kanagawa University, 3-27-1 Rokkakubashi, Kanagawa, Yokohama, Kanagawa 221-8686, Japan [18]Faculty of Science and Technology, Graduate School of Science and Technology, Hirosaki University, 3, Bunkyo, Hirosaki, Aomori 036-8561, Japan [19]Department of Electronic Information Systems, Shibaura Institute of Technology, 307 Fukasaku, Minuma, Saitama 337-8570, Japan [20]School of Advanced Science and Engineering, Waseda University, 3-4-1 Okubo, Shinjuku, Tokyo 169-8555, Japan [21]Okinawa Institute of Science and Technology, 1919-1 Tancha, Onna-son, Kunigami-gun Okinawa 904-0495, Japan [22]Faculty of Engineering, Division of Intelligent Systems Engineering, Yokohama National University, 79-5 Tokiwadai, Hodogaya, Yokohama 240-8501, Japan [23]Faculty of Science, Shinshu University, 3-1-1 Asahi, Matsumoto, Nagano 390-8621, Japan [24]Department of Physics, Graduate School of Science, Tokyo Metropolitan University , 1-1 Minamii-Osawa, Hachioji, Tokyo 192-0397, Japan [25]National Astronomical Observatory of Japan, 2-21-1 Osawa, Mitaka, Tokyo 181-8588, Japan [26]Department of Physical Sciences, College of Science and Engineering, Aoyama Gakuin University, 5-10-1 Fuchinobe, Chuo, Sagamihara, Kanagawa 252-5258, Japan [27]Institute of Particle and Nuclear Studies, High Energy Accelerator Research Organization, 1-1 Oho, Tsukuba, Ibaraki 305-0801, Japan [28]University of Pisa, Polo Fibonacci, Largo B. Pontecorvo, 3 - 56127 Pisa, Italy [29]Department of Electrical and Computer Engineering, National Institute of Technology (KOSEN), Gifu College, 2236-2 Kamimakuwa, Motosu-city, Gifu 501-0495, Japan [30]Center for Research and Exploration in Space Sciences and Technology, NASA/GSFC, Greenbelt, Maryland 20771, USA [31]Department of Astronomy, University of Maryland, College Park, Maryland 20742, USA [32]Department of Physical Sciences, College of Science and Engineering, Ritsumeikan University, Shiga 525-8577, Japan [33]Faculty of Science and Engineering, Global Center for Science and Engineering, Waseda University, 3-4-1 Okubo, Shinjuku, Tokyo 169-8555, Japan [34]Department of Physics and Astronomy, University of Denver, Physics Building, Room 211, 2112 East Wesley Avenue, Denver, Colorado 80208-6900, USA [35]Quantum ICT Advanced Development Center, National Institute of Information and Communications Technology, 4-2-1 Nukui-Kitamachi, Koganei, Tokyo 184-8795, Japan [36]Kavli Institute for Cosmological Physics, The University of Chicago, 5640 South Ellis Avenue, Chicago, IL 60637, USA [37]College of Industrial Technology, Nihon University, 1-2-1 Izumi, Narashino, Chiba 275-8575, Japan [38]Graduate School of Science, Osaka Metropolitan University, Sugimoto, Sumiyoshi, Osaka 558-8585, Japan [39]Nambu Yoichiro Institute for Theoretical and Experimental Physics, Osaka Metropolitan University, Sugimoto, Sumiyoshi, Osaka 558-8585, Japan [40]National Institutes for Quantum and Radiation Science and Technology, 4-9-1 Anagawa, Inage, Chiba 263-8555, Japan [41]Nagoya University, Furo, Chikusa, Nagoya 464-8601, Japan [42]College of Science, Ibaraki University, 2-1-1 Bunkyo, Mito, Ibaraki 310-8512, Japan

PoS(ICRC2025)165